

Joint Detection and Localization of Stealth False Data Injection Attacks in Smart Grids using Graph Neural Networks

Osman Boyaci, Mohammad Rasoul Narimani, Katherine Davis, Muhammad Ismail, Thomas J Overbye, and Erchin Serpedin

Abstract— False data injection attacks (FDIA) are becoming an active avenue of research as such attacks are more frequently encountered in power systems. Contrary to the detection of these attacks, less attention has been paid to identifying the attacked units of the grid. To this end, this work jointly studies detecting and localizing the stealth FDIA in modern power grids. Exploiting the inherent graph topology of power systems as well as the spatial correlations of smart meters’ data, this paper proposes an approach based on the graph neural network (GNN) to identify the presence and location of the FDIA. The proposed approach leverages the auto-regressive moving average (ARMA) type graph convolutional filters which offer better noise robustness and frequency response flexibility compared to the polynomial type graph convolutional filters such as Chebyshev. To the best of our knowledge, this is the first work based on GNN that automatically detects and localizes FDIA in power systems. Extensive simulations and visualizations show that the proposed approach outperforms the available methods in both detection and localization FDIA for different IEEE test systems. Thus, the targeted areas in power grids can be identified and preventive actions can be taken before the attack impacts the grid.

NOMENCLATURE

$P_i + jQ_i$	Complex power injection at bus i .
$P_{ij} + jQ_{ij}$	Complex power flow between bus i and j .
V_i, θ_i	Voltage magnitude and phase angle of bus i .
n, m	Number of buses, number of measurements.
$\mathcal{X} \in \mathbb{R}^n$	State space.
$\mathcal{Z} \in \mathbb{R}^m$	Measurement space.
$\mathbf{x} \in \mathcal{X}$	A state vector.
$\hat{\mathbf{x}} \in \mathcal{X}$	Original state vector without an attack.
$\tilde{\mathbf{x}} \in \mathcal{X}$	False data injected state vector.
$\mathbf{z} \in \mathcal{Z}$	A measurement vector.
$\mathbf{z}_o \in \mathcal{Z}$	Original measurement vector.
$\mathbf{a} \in \mathcal{Z}$	Attack vector.
$\mathbf{z}_a \in \mathcal{Z}$	Attacked measurement vector.
$h(\mathbf{x})$	Nonlinear measurement function at \mathbf{x} .
\mathcal{T}	Attacker’s target area to perform FDI attack.

I. INTRODUCTION

Smart grids integrate Information and Communication Technologies (ICT) into large scale power networks to generate,

O. Boyaci, M. R. Narimani, K. Davis, T. J. Overbye and E. Serpedin are with the Department of Electrical and Computer Engineering, Texas A&M University, College Station, TX 77843 USA (e-mail: {osman.boyaci, narimani, katedavis, overbye, eserpedin}@tamu.edu). M. Ismail is with the Department of Computer Science, Tennessee Tech University, Cookeville, TN 38505 USA (email: mismail@ntech.edu)

This work was supported by NSF under Award Number 1808064. The data that support the findings of this study are available at <https://katedavis.engr.tamu.edu/projects/defenda/>

and distribute electricity more efficiently [1]. Remote Terminal Units (RTUs) and Phasor Measurement Units (PMUs) are utilized to acquire the physical measurements and deliver them to the Supervisory Control and Data Acquisition Systems (SCADAs). Then, the ICT network transfers these measurements to the application level where the power system operators process them and take the necessary actions [2]. As a direct consequence, power system reliability is determined by the accuracy of the steps along this cyber-physical pipeline [3]. Power system state estimation (PSSE) modules employ these measurements to estimate the current operating point of the grid [4] and thus the integrity and trustworthiness of the measurements are crucial for proper operation of power systems. In addition, the accuracy of power system analysis tools such as energy management, contingency and reliability analysis, load and price forecasting, and economic dispatch depends on these measurements. [4]. Thus, power system operation strongly depends on the accuracy of the measurements and the integrity of their flow through the system. Therefore, the smart metering devices represent highly attractive targets for adversaries that try to obstruct the smart grid operation by corrupting the measurements.

By disrupting the integrity of measurement data, false data injection attacks (FDIA) constitute a considerable cyber-physical threat. More specifically, an attacker injects some false data to the measurements in order to mislead the PSSE and force it to converge to another operating point. Since the state of the power system is miscalculated by using these false data, any action taken by the grid operator based on the false operating point can lead to serious physical consequences including systematic problems and failures [5]. In traditional power grids, the largest normalized residual test (LNRT) is employed within the bad data detection (BDD) module along with PSSE to detect the “bad” measurement data [6]. Nevertheless, a false data injected measurement can easily bypass the BDD without any suspicion. In particular, [7] shows that by satisfying the power flow equations, an intruder can create an unobservable (stealth) FDIA and bypass the BDD if s/he has sufficient information about the grid. Various methods have been proposed to alert the grid operator about the presence of the FDIA without providing any information about the attack location [7]. While there has been a great deal of research on detection of FDIA, only a few attempts have been made to localize the attack [8]–[13]. Localizing the attack is crucial for power system operators since they can take preventive action such as isolating the under-attack buses and re-dispatch the system accordingly. Therefore, this paper focuses jointly on detection and localization of the FDIA in

power systems.

A multistage localization algorithm based on graph theory techniques is proposed in [8] to localize the attack at cluster level. Authors in [10] propose physics and learning-based approaches to detect and localize the FDIA in automatic generation control (AGC) in power systems. The physics-based method relies on interaction variables while the learning based approach assumes deep learning. The learning approach exploits the historical Area Control Error (ACE) data, and utilizes a Long Short Term Memory (LSTM) Neural Network (NN) to generate a model to learn the data pattern. Any deviation from the historical normal point is categorized as an attack. A generalized modulation operator that is applied on the states of the system is presented in [11] to localize the FDIA in power systems. The attack location is identified by the grid states that exhibit specific modulation. A Graph Signal Processing (GSP) based approach is developed in [12] to detect and localize the FDIA using the Graph Fourier Transform (GFT), local smoothness, and vertex-frequency energy distribution methods. Authors in [13] present an internal observer-based detection and localization method for FDIA in power systems. They create and assign an interval observer to each measurement device and construct a customized logic localization judgment matrix to detect and localize the FDIA.

Since localization of FDIA is relatively a newer research subject compared to detection of FDIA, the current approaches proposed in literature suffer of some limitations. To begin with, multiple studies use DC based electric grid modeling. Although this linearization greatly simplifies the calculations, it does not capture the actual grid operations [2]. Secondly, the inherent graph topology of the power systems is mostly ignored which restricts the localization accuracy. Thirdly, most of the current works use point wise, random or easily detectable attacks to test their models which do not comprehensively assess the actual performance of their models. Lack of scalability and custom solutions requiring manual labor represent additional limitations of the proposed solutions. For instance, the IEEE 14-bus test case is used as the de facto test system for researchers. Nevertheless, the limited number of components in this system deeply confines the large scale attributes of the proposed models. Lastly, resolution of the localization can be a limiting factor for the current models. In particular, cluster level localization reduces the resolution which hinders the benefits of localization. Thus, some approaches design a separate detector for each bus to provide a higher resolution. However, such approaches highly increase the model complexity, and thus reduce their suitability for real world applications.

In general, there are two main approaches to detect and localize the FDIA: model-based and data driven methods. In the model-based methods [8], [9], [11]–[13], a model for the system is built and its parameters are estimated to detect the FDIA. Since there is no training, these methods do not require the historical data. However, the detection delays, scalability issues and threshold tuning steps can limit the performance and usability of the model-based approaches [14]. Conversely, the data-driven methods [10] are system independent and require historical data and a training procedure. However, they provide scalability and real time compatibility due to the excessive training [14]. Data driven methods, machine learning (ML), in particular, offer superior performances to detect FDIA in

power systems as the historical datasets are growing.

The architecture of a ML algorithm is determined by the structure of the dataset samples to capture the patterns in it [15]. For instance, a recurrent neural network (RNN) architecture is well suited to recognize the patterns in the natural language processing (NLP) tasks such as sequence to sequence language modeling and machine translations. Similarly, convolutional neural networks (CNN) are more pertinent to image and video processing tasks since sliding kernels can easily capture the pixel locality in the Euclidean space [16]. Nevertheless, graph structural data such as social networks, traffic networks, and electric grid networks can not be modeled efficiently in the Euclidean space and require graph-type architectures.

Graph Signal Processing (GSP) has emerged in the past few years to deal with the data in non-Euclidean spaces [17]. A few researchers designed spectral filters to detect and localize the FDIA [11], [12] using GSP. However, manual tailoring of the filters and detection thresholds substantially limits the applicability and efficiency of this approach. Conversely, the Graph Neural Network (GNN), as a data-driven counterpart of the GSP, eliminates the custom design steps and provides an end-to-end design that exploits the spatial locality dictated by the historical data. Toward this end, we use GNN for modeling the smart grid network for detecting and localizing the FDIA.

The contributions of this work are outlined as follows:

- To accurately model the underlying physical system, we use the full AC power flow equations instead of the DC approximation.
- To properly capture the spatial correlations of the smart grid data collected from the cyber system, we propose a topology aware GNN model for training our model.
- To precisely test our proposed method, we generate 1 year of dataset with 15 minute intervals using the stealth FDIA generation algorithm developed in our previous paper [18] that accurately mimics the distribution of smart grid data in order to be undetectable to the traditional BDD methods.
- To specifically determine the location(s) of the attacks, we developed a joint method for detecting and localizing the attacks which returns $n + 1$ binary labels that indicate the presence of the attacks for the whole grid and for each bus separately.

This rest of this paper is organized as follows. Section II presents the problem formulation. Section III proposes the approach for the joint detection and localization of FDIA. Numerical results are presented in Section IV. Section V concludes the paper.

II. PROBLEM FORMULATION

The system state \mathbf{x} (voltage magnitude V_i and voltage angle θ_i at each bus) is estimated using the PSSE module. The PSSE iteratively solves the optimization problem in (1) phrased as a weighted least squares estimation (WLSE) of the system states using the complex power measurements \mathbf{z} collected in noisy conditions by RTUs and PMUs:

$$\hat{\mathbf{x}} = \min_{\mathbf{x}} (\mathbf{z} - h(\mathbf{x}))^T \mathbf{R}^{-1} (\mathbf{z} - h(\mathbf{x})), \quad (1)$$

where \mathbf{R} represents measurements' error covariance matrix and \mathbf{z} includes active/reactive powers injections at buses (P_i, Q_i) and power flows on branches (P_{ij}, Q_{ij}).

FDIA aim to deceive the PSSE by deliberately injecting false data \mathbf{a} into some of the original measurement \mathbf{z}_o in such a way that the state vector \mathbf{x} converges to another point in the state space of the system. Formally,

$$\mathbf{z}_o = h(\hat{\mathbf{x}}), \quad \mathbf{z}_a = \mathbf{z}_o + \mathbf{a} = h(\tilde{\mathbf{x}}) \quad (2)$$

which means if an adversary can design the FDIA \mathbf{a} such that $\mathbf{a} = h(\tilde{\mathbf{x}}) - h(\hat{\mathbf{x}})$, it can easily change the system state from $\hat{\mathbf{x}}$ to $\tilde{\mathbf{x}}$ without being detected by the LNRT based traditional BDD systems.

In general, an adversary tries to change specific measurement(s) in the power system in order to maximize the damage to the grid and at the same time minimize the probability of being detected. To this end, s/he alters some other measurement(s) connected to the targeted meter(s) since each x relates to multiple z through $z = h(x)$. In order to reflect this constraint and to be realistic, we assume that an adversary targets a specific area of grid represented by \mathcal{T} and crafts the attack vector \mathbf{a} by changing the measurements denoted by \mathcal{T}_z to spoil the state variables represented by \mathcal{T}_x in this area.

The grid operator, in contrast, aims to detect those attacks and localize the attacked buses if there are any. Therefore, we formulate the FDIA detecting and localization problem as a *multi-label* classification task where each bus has a binary label indicating the presence of attack with true label 1. We also reserve an extra binary label for the whole grid to denote the attack presence with true label 1. Fig. 1 clarifies the proposed multi-label classification approach by depicting the actual and predicted under attack buses for an exemplary attack on the IEEE 14-bus test system.

III. JOINT DETECTION AND LOCALIZATION OF FDIA

Connected, undirected and weighted graph $\mathcal{G} = (\mathcal{V}, \mathcal{E}, \mathbf{W})$ having a finite set of vertices \mathcal{V} with $|\mathcal{V}| = n$, a finite set of edges \mathcal{E} , and a weighted adjacency matrix $\mathbf{W} \in \mathbb{R}^{n \times n}$ can be used to effectively represent a smart power grid [17]. In this representation, buses correspond to vertices \mathcal{V} , branches and transformers corresponds to edges \mathcal{E} and line admittances correspond to \mathbf{W} . Similarly, a signal or a function $f: \mathcal{V} \rightarrow \mathbb{R}$

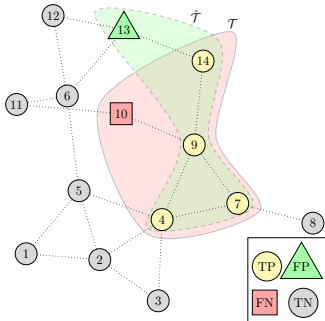


Fig. 1. Visualization of an attack and its prediction on the example IEEE 14 bus system where the actual $\mathcal{T} = \{4, 7, 9, 10, 14\}$ and predicted $\hat{\mathcal{T}} = \{4, 7, 9, 13, 14\}$ areas are enclosed with the solid red and dashed green surfaces, respectively. True positives $\mathcal{T} \cap \hat{\mathcal{T}} = \{4, 7, 9, 14\}$, false positives $\mathcal{T}' \cap \hat{\mathcal{T}} = \{13\}$, false negatives $\mathcal{T} \cap \hat{\mathcal{T}}' = \{10\}$, and true negatives $\mathcal{T}' \cap \hat{\mathcal{T}}' = \{1, 2, 3, 5, 8, 6, 11, 12\}$ are represented by yellow circles, green triangles, red squares, and black circles, respectively. In this example, presence of the attack is correctly predicted. Nevertheless, attack to the bus 10 is missed and bus 13 is falsely alarmed even though it is not under attack.

in \mathcal{G} is represented by a vector $\mathbf{f} \in \mathbb{R}^n$, where the element i of the vector corresponds to a scalar at the vertex $i \in \mathcal{V}$.

A. Spectral Graph Filters

In spectral graph theory, the normalized Laplacian operator $\mathbf{L} = \mathbf{I}_n - \mathbf{D}^{-1/2} \mathbf{W} \mathbf{D}^{-1/2} = \mathbf{U} \mathbf{\Lambda} \mathbf{U}^T \in \mathbb{R}^{n \times n}$ plays an important role for graph \mathcal{G} . The columns of matrix $\mathbf{U} = [\mathbf{u}_1, \dots, \mathbf{u}_n] \in \mathbb{R}^{n \times n}$ store the n orthonormal eigenvectors and stand for the graph Fourier basis. Diagonal matrix $\mathbf{\Lambda} = \text{diag}([\lambda_1, \dots, \lambda_n]) \in \mathbb{R}^{n \times n}$ captures the n eigenvalues representing the frequencies of graph spectral domain [17]. Analogously to the classical Fourier Transform, Graph Fourier Transform (GFT) transforms a vertex domain signal into the graph spectral domain: the forward and inverse GFT are defined by $\tilde{\mathbf{X}} = \mathbf{U}^T \mathbf{X}$, and $\mathbf{X} = \mathbf{U} \tilde{\mathbf{X}}$, where \mathbf{X} and $\tilde{\mathbf{X}} \in \mathbb{R}^{n \times f}$ denote the vertex and spectral domain signals with f features at each node, respectively [17]. Similar to the classical signal processing, \mathbf{X} is filtered by h

$$\mathbf{Y} = h * \mathbf{X} = h(\mathbf{L}) \mathbf{X} = \mathbf{U} h(\mathbf{\Lambda}) \mathbf{U}^T \mathbf{X} \quad (3)$$

by first converting the vertex domain signal into the spectral domain using the forward GFT, then scaling the Fourier components by $h(\mathbf{\Lambda}) = \text{diag}[h(\lambda_1), \dots, h(\lambda_n)]$, and finally reverting it back to the vertex domain by the inverse GFT [17]. Nonetheless, this spectral filtering is not spatially localized since each λ_i is processed for each node and its computational complexity is high due to eigendecomposition of \mathbf{L} and the matrix multiplications with \mathbf{U} and \mathbf{U}^T .

B. Polynomial FIR Graph Filters

To localize spectral filters and reduce their complexity, polynomial spatial filters $h_{POLY}(\lambda) = \sum_{k=0}^K a_k \lambda^k$ are proposed to approximate the required filter response [19]. Since only K -hop neighbors of v are considered to calculate the filter response at each $v \in \mathcal{V}$, they are K -localized. In fact, they implement the weighted Moving Average (MA) filtering in the form of Finite Impulse Response (FIR) [20]. Besides, they do not require eigendecomposition of \mathbf{L} since their parameters are free from the spectrum of λ [19].

Chebyshev polynomial approximation [21] is one of the preferred methods in signal processing due to their fast computation since they are generated via a recursion and not a convolution [22]. In fact, the Chebyshev polynomial of the first kind $T_k(x)$ can be computed recursively $T_k(x) = 2xT_{k-1}(x) - T_{k-2}(x)$ where $T_0(x) = 1$ and $T_1(x) = x$ [21]. Thus, a filter h can be approximated by a truncated expansion of Chebyshev polynomials T_k , up order $K-1$. So, \mathbf{X} can be filtered:

$$\mathbf{Y} = h * \mathbf{X} = h(\mathbf{L}) \mathbf{X} = \sum_{k=0}^{K-1} a_k T_k(\tilde{\mathbf{L}}) \mathbf{X} \quad (4)$$

where $T_k(\tilde{\mathbf{L}}) \in \mathbb{R}^{n \times n}$ is the Chebyshev polynomial of order k evaluated at the scaled Laplacian $\tilde{\mathbf{L}} = 2\mathbf{L}/\lambda_{max} - \mathbf{I}_n$ [19] and $\mathbf{a} \in \mathbb{R}^K$ is a vector of Chebyshev coefficients. In spite of the fact that MA type polynomial filters are fast and localized, they often require high-degree polynomials to capture the time varying graph signals such as power system data [23]. This increases the MA polynomial filters sensitivity to noise, and as a consequence it deteriorates their generalization power [24].

Besides, the MA structure of the polynomial filters restricts their ability to adapt to sharp transitions in the frequency response [23].

C. Rational IIR Graph Filters

To circumvent these problems, distributed auto-regressive moving average (ARMA) type graph filters that provide better approximations to sudden changes in the frequency response in comparison with the MA polynomial type filters due to their rational filter composition are proposed in [23] and [25]. A potential building block of K -order ARMA graph filters may start with a first order recursive ARMA-1 filter:

$$\mathbf{Y}^{t+1} = a\tilde{\mathbf{L}}\mathbf{Y}^t + b\mathbf{X}, \quad (5)$$

where \mathbf{Y}^t is the filter output at iteration t , a and b are arbitrary coefficients, and modified Laplacian $\tilde{\mathbf{L}} = \frac{\lambda_{max} - \lambda_{min}}{2} \mathbf{I}_n - \mathbf{L}$ represents a linear translation of \mathbf{L} with same eigenvectors as \mathbf{L} and shifted eigenvalues $\tilde{\lambda}_n = \frac{\lambda_{max} - \lambda_{min}}{2} - \lambda_n$ relative to those of \mathbf{L} . According to the Theorem (1) in [26], Eq. (5) converges regardless of \mathbf{Y}^0 and \mathbf{L} values and its frequency response is given by $h_{ARMA_1}(\tilde{\lambda}_n) = \frac{b}{1 - a\tilde{\lambda}_n}$. Besides, aggregating K parallel ARMA₁ filters leads to ARMA_K filters with rational frequency response $h_{ARMA_K}(\tilde{\lambda}_n) = \sum_{k=1}^K \frac{b_k}{1 - a_k\tilde{\lambda}_n}$ with a $K - 1$ and K order polynomials in its numerator and denominator, respectively.

Eq. (5) provides a useful distributed filter realization. At each iteration t , each node i revises its output $\mathbf{Y}_i^t \in \mathbb{R}^{n \times c_{out}}$ with a linear combination of its input $\mathbf{X}_i \in \mathbb{R}^{n \times c_{in}}$ and its adjacent nodes' outputs \mathbf{Y}_j^{t-1} , where c_{in} and c_{out} denote the number of channels in the input and the output tensors, respectively. In fact, it can be implemented as a neural network layer if we unroll the recursion into T fixed iterations:

$$\mathbf{Y}^{t+1} = \tilde{\mathbf{L}}\mathbf{Y}^t\boldsymbol{\alpha} + \mathbf{X}\boldsymbol{\beta} + \boldsymbol{\theta} \quad (6)$$

where $\boldsymbol{\alpha} \in \mathbb{R}^{c_{out} \times c_{out}}$, $\boldsymbol{\beta} \in \mathbb{R}^{c_{in} \times c_{out}}$, and $\boldsymbol{\theta} \in \mathbb{R}^{c_{out}}$ are trainable weights. Besides, since $0 \leq \lambda_{min} \leq \lambda_{max} \leq 2$, the modified Laplacian can be simplified to $\tilde{\mathbf{L}} = \mathbf{I}_n - \mathbf{L}$ for $\lambda_{min} = 0$, and $\lambda_{max} = 2$ [24]. Also, their K -order version ARMA_K filters can be realized by averaging K parallel ARMA₁ filters with $\mathbf{Y} = \frac{1}{K} \sum_{k=1}^K \mathbf{Y}_K^T$. For detailed analysis and justifications, please refer to [23]–[25].

D. Architecture of the Proposed Joint Detector & Localizer

The proposed joint detector and localizer consist of one input layer to represent complex bus power injections, $L - 1$ hidden ARMA_K layers to extract spatial features, one dense layer to predict the probability of attack at each node, and one output layer to return an extra bit to indicate the probability of attack at the graph level. Its architecture is depicted in Fig. 2 for l_3 with a small graph having $n = 5$.

In this multi-layer GNN model, the input tensor $[P_i, Q_i]$ is given by $\mathbf{X}^0 \in \mathbb{R}^{n \times 2}$, the output tensor of hidden layer l is denoted by $\mathbf{X}^l \in \mathbb{R}^{n \times c_l}$, and model outputs are denoted by $\mathbf{Y} \in \mathbb{R}^n$ and $S \in \mathbb{R}$ to indicate the location and the presence of the attack, respectively, where c_l represents the number of channels in layer l for $1 \leq l \leq L$. In particular, while an ARMA- K layer takes $\mathbf{X}^{l-1} \in \mathbb{R}^{n \times c_{l-1}}$ as input and produces $\mathbf{X}^l \in \mathbb{R}^{n \times c_l}$ as output in layer l , the dense layer propagates the information to the whole graph and outputs

the probability of the attack at the node level with $\mathbf{Y} \in \mathbb{R}^n$ for localization. Finally, the output layer detects the attack at the graph level by $S = \max(\mathbf{Y}) \in \mathbb{R}$ and outputs it with \mathbf{Y} . Note that the last ARMA- K layer's output channel is selected as one in order to have one feature for each $v \in \mathcal{V}$. In addition, ReLU activation is used at the end of each ARMA- K layer to increase the model's nonlinear modeling ability, whereas sigmoid is employed to transform the outputs to probabilities.

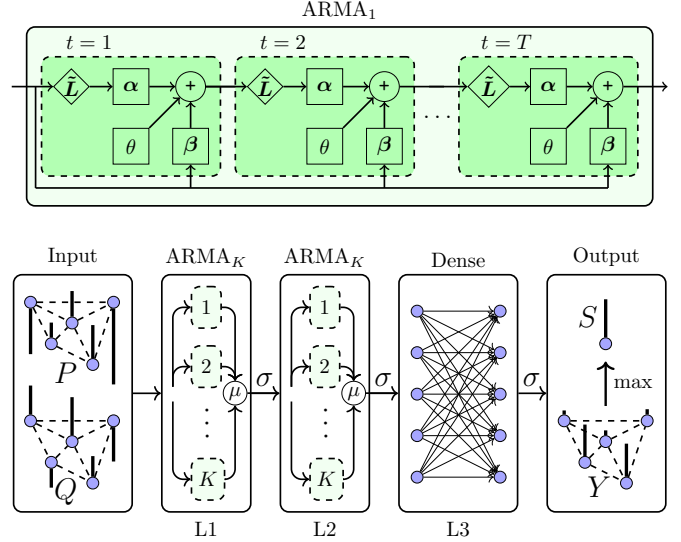


Fig. 2. Architecture of the proposed detector and localizer with three hidden layers where each ARMA_K layer consists of K parallel ARMA₁ as a building block. While complex power injections P, Q and predicted attack probabilities \mathbf{Y}, S at the node and graph level are visualized with thick bars at each node, activation and mean value functions are represented with σ and μ , respectively.

IV. EXPERIMENTAL RESULTS

A. Data Generation

Due to the privacy concerns, there is no preexisting publicly available dataset to train and evaluate the proposed models against FDIA. Thus, as a first step, we generate a realistic dataset following the Algorithm 1 in our previous work [18] for the IEEE 14-, 118-, and 300-bus standard test cases using 15-minute intervals load profile of Southern Texas [27]. Then, we apply stealth FDIA to the samples using Tensorflow [28] and our constrained optimization based stealth FDIA generation method explained thoroughly in Algorithm 2 in [18]. The final dataset spans one whole year of data having 96 sample/day * 365 day = 35040 samples which has complex power measurements, complex bus voltages, and $n + 1$ binary labels to indicate the true labels for each bus and the whole grid at each timestamp. To visualize the attacked meters and their locations, attack ratios are plotted along the samples in percentages for IEEE 118- and 300-bus test cases in Figs. 3a, and 3a, respectively. While generators and zero injections buses are never targeted by the attacker since it would be risky to inject the false data, some nodes, especially the ones that have high connections, are included in the target area by the attacker more than 50% percent of the attacks. Besides, attack ratio at the grid level is measured as 50%, 47%, and 36% for IEEE 14-, 118-, and 300-bus test systems, respectively. Interested readers are directed to Sections III-A and IV-A

of our previous work [18] for detailed analysis of the data generation steps.

B. Detecting & Localizing the Attacks

In our model, we only employ the power injection to the buses in the system (i.e., P_i and Q_i) and neglect the power flows in the lines (i.e., P_{ij} , and Q_{ij}) as well as the voltage magnitude and angle of buses (i.e., V_i , and θ_i). Since we do not use the PMU data in this paper we have to solve the PSSE to calculate the voltage magnitude and angle of the buses which delays the detection. However, the voltage magnitude and angle of buses are related to the power flow in lines through the power flow equation (i.e., P_{ij} , and Q_{ij}). Thus, in order to overcome the overfitting problems [15], the voltage magnitude and angle of buses are ignored in this paper. Besides, since power injection to buses is represented by the summation of power flows that inject/withdraw into/from the bus, we neglect power flow in the lines.

We select $W = |Y_{bus}|$ to calculate \tilde{L} and feed the ARMA_K layers. In the pre-processing phase, we split the one year data into 3 sections: the first 8 months for training, the next 2 months for validating and hyper-parameter tuning, and the last 2 months for testing the proposed models. Then, we standardize each split separately, with a zero mean and a standard deviation of one, to have a faster and smoother learning process [15].

All free unknown parameters defined in the model are computed by a multi-label supervised training using the binary cross-entropy loss. Training samples are fed into the model as mini batches of 128 samples with 256 maximum number of epochs. In addition, we employ early stopping criteria where 16 epochs are tolerated without any improvement less than e^{-4} in the validation set's cross entropy loss. All the implementations were carried out in Python 3.8 using the Pandapower [29], Sklearn [30], t-SNE [31], and Tensorflow [28] libraries on Intel i9-8950 HK CPU 2.90GHz with NVIDIA GeForce RTX 2070 GPU.

For performance evaluation we use detection rate $DR = \frac{TP}{TP+FN}$, false alarm rate $FA = \frac{FP}{FP+TN}$, and F1 score $F1 = \frac{2*TP}{2*TP+FP+FN}$, where TP , FP , TN , and FN represent true positives, false positives, true negatives, and false negatives, respectively [15]. Since $n + 1$ binary labels are predicted at each time-step, we used sample-wise mean of each metric to compare the model. In addition, to overcome the division by zero problem at the timesteps when there is no attack at all, we assumed $DR=1$, $FA=0$, and $F1=1$ if all the labels are correctly predicted as not attacked. Otherwise, even there is one mismatch, we assigned $DR=0$, $FA=1$, and $F1=0$.

Although they are proposed mostly for detection, we also implement other available methods in the literature suitable for the multi-label classification task such as Decision Tree (DT) [32], K-Nearest Neighbor (KNN) [33], Multi Layer Perceptron (MLP) [34], Recurrent Neural Network (RNN) [10], Convolutional Neural Network (CNN) [33], and Chebyshev GNN (CHEB) [18] based FDIA detectors to compare our ARMA GNN model. We train, validate and test these models similarly to our proposed model using our dataset.

In Table I, detection performance of the models for each test system is tabulated as percentages, where the first and second best performances in each column are marked with bold and italic fonts, respectively. In addition, we underline the

TABLE I
DETECTION RESULTS.

System	IEEE-14			IEEE-118			IEEE-300		
	DR	FA	F1	DR	FA	F1	DR	FA	F1
DT	93.21	16.87	88.78	93.48	17.70	87.59	94.80	4.51	93.91
KNN	87.27	0.89	92.76	53.21	0.19	69.36	15.63	0.03	27.03
MLP	96.08	6.08	95.07	97.56	1.13	98.13	95.73	0.67	97.29
RNN	95.73	6.15	94.86	98.21	7.11	95.25	<i>98.94</i>	7.40	93.98
CNN	95.39	3.78	95.80	98.40	4.46	96.74	99.82	6.33	95.17
CHEB	95.43	3.30	<i>96.05</i>	98.07	1.23	<i>98.34</i>	99.78	3.22	<i>97.42</i>
ARMA	<i>94.57</i>	<i>1.44</i>	96.50	<i>98.25</i>	<i>0.52</i>	98.83	99.82	<i>0.53</i>	99.50

metrics of proposed ARMA model for easy visualization. For the 14-bus system, while MLP gives the best DR at 96.08%, KNN yields the lowest FA at 0.89%. Nevertheless, their overall performances are not as good as ARMA since KNN could only detect 87.27% of the attacks, whereas MLP falsely predicted no-attacks as attacks with 6.08%. In contrast, ARMA outperforms all the other models with overall score of 96.50% and the difference relative to the second best model CHEB is measured as 0.45% in F1 score. As for IEEE-118, CNN takes the lead with 98.40% in DR and KNN gives the minimum FA with 0.19%. However, similar to the IEEE-14, ARMA wins in F1 score with 98.83% with a 0.49% difference from that of CHEB. Lastly for IEEE-300 testbed, CNN, and ARMA reach the same best performance 99.82% in DR, yet with 0.53% FA rate and 99.50% F1 overall score, ARMA outperforms the others with a minimum of 2.08% in F1 difference. In addition, 0.03% FA could not make KNN competitive due to the highly poor 15.63% detection performance.

Since localization is a multi-label classification problem, we evaluate it in both possible ways: (i) sample-wise evaluation where each sample at a fixed time-step is treated individually along the buses, and (ii) node-wise evaluation where each bus is evaluated separately along the samples. Mean value of sample-wise localization results are listed in Table II. It is seen from the Table II that even though KNN yields the lowest FA, its DR is not compatible with the others. DT, in contrast, fails due to its highest FA score. Graph based models CHEB and ARMA clearly exceed other models. ARMA, in particular, yields the best results 93.35%, 95.22%, and 97.02% in F1 score for IEEE 14-, 118- and 300-bus system, respectively.

Fig. 3, in contrast, demonstrates the bus-wise localization results of the proposed model for IEEE-118 and 300-bus systems where each bus is depicted with a color to indicate its F1 score in percentage. Their F1 values deviate between 68.86% - 100%, and 66.21% - 100% with the mean values of

TABLE II
SAMPLE-WISE LOCALIZATION RESULTS.

System	IEEE-14			IEEE-118			IEEE-300		
	DR	FA	F1	DR	FA	F1	DR	FA	F1
DT	84.00	4.69	83.25	77.97	3.88	76.08	88.17	2.26	87.22
KNN	90.43	1.35	90.21	70.38	0.30	72.26	64.71	0.03	65.43
MLP	<i>93.80</i>	1.69	92.90	95.78	1.34	93.82	92.6	1.25	91.91
RNN	93.26	2.27	92.18	93.01	1.12	91.76	92.65	1.07	91.80
CNN	93.27	2.04	92.66	93.34	0.80	92.97	94.72	0.98	93.15
CHEB	93.43	<i>1.62</i>	<i>93.09</i>	95.20	0.94	<i>94.37</i>	96.53	0.96	95.08
ARMA	93.93	1.96	93.35	96.44	0.97	95.22	97.84	<i>0.74</i>	97.02

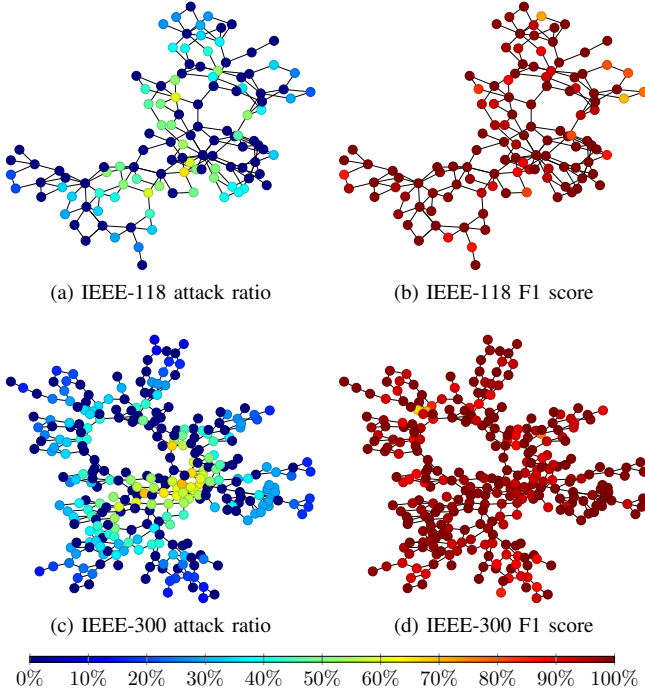


Fig. 3. Bus-wise attack ratios are localization results in percentage. First and second row demonstrate the frequency and detection score of the attacks for each bus along the samples. Note that while some load buses located in the center of the grid are included in \mathcal{T} frequently, generators and zero-injection buses are never attacked due to their high detection risks. Except a few nodes, F1 score of buses exceed 95%.

96.46% and 96.95% for the IEEE-118 and 300-bus systems, respectively.

Analyzing the performance in terms of detecting and localizing FDIA in power systems of different algorithms highlights that, in general, because of their high modeling capability, models from NN family performs better than DT and KNN. Nevertheless, the performance of MLP and RNN is not satisfactory compared to the convolutional NN such as CNN, CHEB, and ARMA since they ignore the locality of the features. From the convolutional architectures, CNN clearly falls behind the GNN models because spatial locality of the smart grid can not be modeled in the Euclidean space and requires graph type architectures such as CHEB and ARMA. As for GNN family, ARMA outperforms CHEB due to the fact that (i) rational graph filters implemented using the ARMA architecture provide more flexible frequency responses, and (ii) they are more robust to noise and time deviations when compared to the polynomial filters such as CHEB [23], [25]. It is also observed that the performance differences increase in larger graphs.

C. Hyper-parameter optimization of the models

Model hyper-parameters are tuned with Sklearn [30] and Keras-tuner [35] Python libraries by using Bayesian optimization techniques. Models are trained on the training set and their hyper-parameters are optimized on the validation set for each IEEE test systems for 100 trials. Finally, models with optimal parameters in terms of the validation set performance are saved and their results are tabulated in Table I and II. Table III shows

the hyper-parameter set and the optimal hyper-parameters for each model and test system.

TABLE III
OPTIMIZED MODEL HYPER-PARAMETERS.

model	param	options	IEEE-14	IEEE-118	IEEE-300
DT	criterion	{gini, entropy}	entropy	entropy	entropy
	min. split	{2, 3, ..., 8}	2	2	2
	max. depth	{1, 2, ..., 64}	64	60	64
	features	{sqrt, log2}	log2	log2	sqrt
KNN	algorithm	{ball, kd}	kd	ball	kd
	neighbors	{3, 5, ..., 9}	3	3	3
	leaf size	{4, 5, ..., 64}	4	64	56
	p	{1, 2, 3, 4}	3	1	1
MLP	layers	{1, 2, 3}	2	3	2
	units	{16, 32, 64, 128}	32	64	128
RNN	layers	{1, 2, 3}	3	3	3
	units	{16, 32, 64, 128}	32	32	32
CNN	layers	{1, 2, 3}	2	2	2
	units	{16, 32, 64, 128}	128	128	64
	K	{2, 3, 4}	2	4	3
CHEB	layers	{1, 2, 3}	3	2	3
	units	{16, 32, 64, 128}	32	64	32
	K	{2, 3, 4}	4	2	4
ARMA	layers	{1, 2, 3}	3	2	3
	units	{16, 32, 64, 128}	32	16	16
	K	{2, 3, 4}	2	3	4
	iteration	{2, 3, 4}	4	4	2

D. Visualization of intermediate layers with t-SNE

To compare the proposed model with the existing approaches, we analyze and visualize the intermediate layers of the proposed models. Nevertheless, high dimensionality of the data severely limits examining them. Besides, examining a specific feature of a bus does not provide enough information to fully comprehend how the model processes the grid. Thus, we transform layer outputs by using the t-distributed stochastic neighbor embedding (t-SNE), which is a nonlinear dimensionality reduction technique to visualize the high dimensional data in two or three dimensional spaces [31]. By iteratively minimizing the Kullback-Leibler divergence between the probability distributions representing the sample similarities in the original and mapped spaces, it projects samples into the low dimensional space. Thus, it preserves the structure of the data and enables visualizing the data in a lower dimension [31].

To better depict the samples after the projection, we encode class and time information of the sample with RGB colors. Namely, binary true and predicted labels are encoded with red (R) and green (G) colors, respectively. In addition, blue (B) color indicates the 15-minute interval of the day. The encoding scheme can be seen in Fig. 4a, where component B simply “modulates” the index of the sample in a day. For instance, the color of a falsely detected sample (FP) changes from green (RGB=[0,1,0]) to cyan (RGB=[0,1,1]) with time. Before embedding, the daily load profile used for generating test data are given in Fig. 4b to illustrate the color gradient.

Due to the space limitation, only models trained for IEEE-300 bus system are analyzed in two dimensions (2D) with test data having $60 * 96 = 5760$ samples. Embedding of input data $[P, Q] = X \in \mathbb{R}^{300 \times 2}$ is plotted in Fig. 4c, where a dominating daily profile similar to the Fig. 4b can be seen from the smooth transition from the lower left (darker) to the upper right (lighter) samples. Moreover, the close proximity between

blue and yellow gradients indicates that the attacked samples preserve similarity to their non-attacked samples due to the stealth attack strategy. Fig. 4d shows the embedding of true output $Y \in \mathbb{R}^{300}$ where non-attacked samples clustered in the middle and attacked samples are scattered around them. This is not surprising since non-attacked samples are all formed from 0s and attacked samples include 1s in their corresponding labels to indicate the attacked bus.

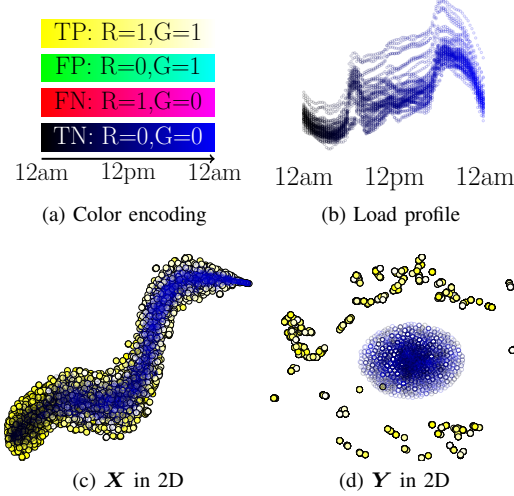


Fig. 4. Color encoding, load profile, and embedded input and output data for IEEE-300 bus system.

Fig. 5 demonstrates the embedding of layer l 's output where each model takes X (Fig. 4c) as input, transforms it in the hidden layers, and tries to predict Y (Fig. 4d) as output. The number of TP, FP, FN, and TN samples are given under the model name with the same color encoding used in Fig. 4a. MLP clearly falls behind the other approaches due to the FNs scattered all around. For instance, unlike other approaches, MLP misses easily detectable 3 attacked samples in l_2 very close to the TP cluster and it maps many FNs nearby to the TNs placed at the lower part of its last layer. RNN, in contrast to the MLP, reduces FN samples. However, in l_2 , it falsely maps many non-attacked samples adjacent to the attacked samples which yields high number of FPs. In addition, like the MLP, it falsely predicts multiple non-attacked clusters in its final layer. Contrarily, CNN, is one of the best models in terms of FN number. Yet, it “destroys” the structure of data in l_1 which brings significant number of FPs. For instance, plenty of non-attacked samples are considered as attacked samples in l_3 even though they are located at the border of non-attacked sample cluster. We believe it is due to the fact that CNN tries to capture the correlations of a non-Euclidean data in an Euclidean space and samples from different classes may look alike the same in that space. Due to their inherent graph architecture, CHEB and ARMA yield better results since they both consider the “structure” of the data within X in their graph convolutional layers. However, CHEB misses one more attack and yields almost 6 times FP samples compared to the ARMA. For instance, a non-attacked sample in the south center of l_4 is falsely regarded as an attack, like the CNN did for l_3 , due to close mapping to an attacked cluster. Conversely, our proposed model gives the lowest number of FP and FN due to its rational graph convolutional filters. Note that no sample is mapped in the vicinity of attacked samples unlike the other models. Besides, only ARMA outputs a highly similar pattern

to Y : a non-attacked sample cluster in the center and attacked samples distributed around it.

V. CONCLUSION

This work proposed a GNN based model by integrating the underlying graph topology of the grid and spacial correlations of its measurement data to jointly detect and localize the stealth FDIA in power systems while the full AC power flow equations are employed to address the physics of the network. Adopting rational ARMA graph convolutions in its hidden layers, the proposed model is more robust to noise and deviations in time. The proposed model is also more flexible in frequency response compared to MA polynomial graph convolutions, e.g., Chebyshev graph convolution. Simulations performed on various standard test systems confirm that the performance of the proposed model in detecting FDIA exceeds the performance of the state of the art CHEB [18] by 0.45%, 0.49%, and 2.08%, for IEEE 14-, 118-, and 300-bus, respectively. The proposed model also outperforms the CHEB model in localizing the attacks (i.e., F1 score) by 0.24%, 0.85%, and 1.96% for the same above mentioned test systems, respectively. Furthermore, visualizing the intermediate layers for different approaches including those in literature corroborates the supremacy of the proposed model in detecting FDIA.

REFERENCES

- [1] X. Yu and Y. Xue, “Smart grids: A cyber-physical systems perspective,” *Proceedings of the IEEE*, vol. 104, no. 5, pp. 1058–1070, 2016.
- [2] K. R. Davis, K. L. Morrow, R. Bobba, and E. Heine, “Power flow cyber attacks and perturbation-based defense,” in *2012 IEEE Third International Conference on Smart Grid Communications (SmartGridComm)*. IEEE, 2012, pp. 342–347.
- [3] S. Sridhar, A. Hahn, and M. Govindarasu, “Cyber-physical system security for the electric power grid,” *Proceedings of the IEEE*, vol. 100, no. 1, pp. 210–224, 2011.
- [4] G. B. Giannakis, V. Kekatos, N. Gatsis, S.-J. Kim, H. Zhu, and B. F. Wollenberg, “Monitoring and optimization for power grids: A signal processing perspective,” *IEEE Signal Processing Magazine*, vol. 30, no. 5, pp. 107–128, 2013.
- [5] G. Liang, J. Zhao, F. Luo, S. R. Weller, and Z. Y. Dong, “A review of false data injection attacks against modern power systems,” *IEEE Transactions on Smart Grid*, vol. 8, no. 4, pp. 1630–1638, 2016.
- [6] A. Abur and A. Expósito, *Power System State Estimation: Theory and Implementation*, ser. Power Engineering (Willis). CRC Press, 2004. [Online]. Available: https://books.google.com/books?id=NQhbtFC6_40C
- [7] Y. Liu, P. Ning, and M. K. Reiter, “False data injection attacks against state estimation in electric power grids,” *ACM Transactions on Information and System Security (TISSEC)*, vol. 14, no. 1, pp. 1–33, 2011.
- [8] T. R. Nudell, S. Nabavi, and A. Chakraborty, “A real-time attack localization algorithm for large power system networks using graph-theoretic techniques,” *IEEE Transactions on Smart Grid*, vol. 6, no. 5, pp. 2551–2559, 2015.
- [9] M. Khalaf, A. Youssef, and E. El-Saadany, “Joint detection and mitigation of false data injection attacks in agc systems,” *IEEE Transactions on Smart Grid*, vol. 10, no. 5, pp. 4985–4995, 2018.
- [10] A. Jevtic, F. Zhang, Q. Li, and M. Ilic, “Physics-and learning-based detection and localization of false data injections in automatic generation control,” *IFAC-PapersOnLine*, vol. 51, no. 28, pp. 702–707, 2018.
- [11] E. Drayer and T. Routtenberg, “Cyber attack localization in smart grids by graph modulation (brief announcement),” in *International Symposium on Cyber Security Cryptography and Machine Learning*. Springer, 2019, pp. 97–100.
- [12] M. A. Hasnat and M. Rahnamay-Naeini, “Detection and locating cyber and physical stresses in smart grids using graph signal processing,” *arXiv preprint arXiv:2006.06095*, 2020.
- [13] X. Luo, Y. Li, X. Wang, and X. Guan, “Interval observer-based detection and localization against false data injection attack in smart grids,” *IEEE Internet of Things Journal*, vol. 8, no. 2, pp. 657–671, 2020.
- [14] A. S. Musleh, G. Chen, and Z. Y. Dong, “A survey on the detection algorithms for false data injection attacks in smart grids,” *IEEE Transactions on Smart Grid*, vol. 11, no. 3, pp. 2218–2234, 2019.

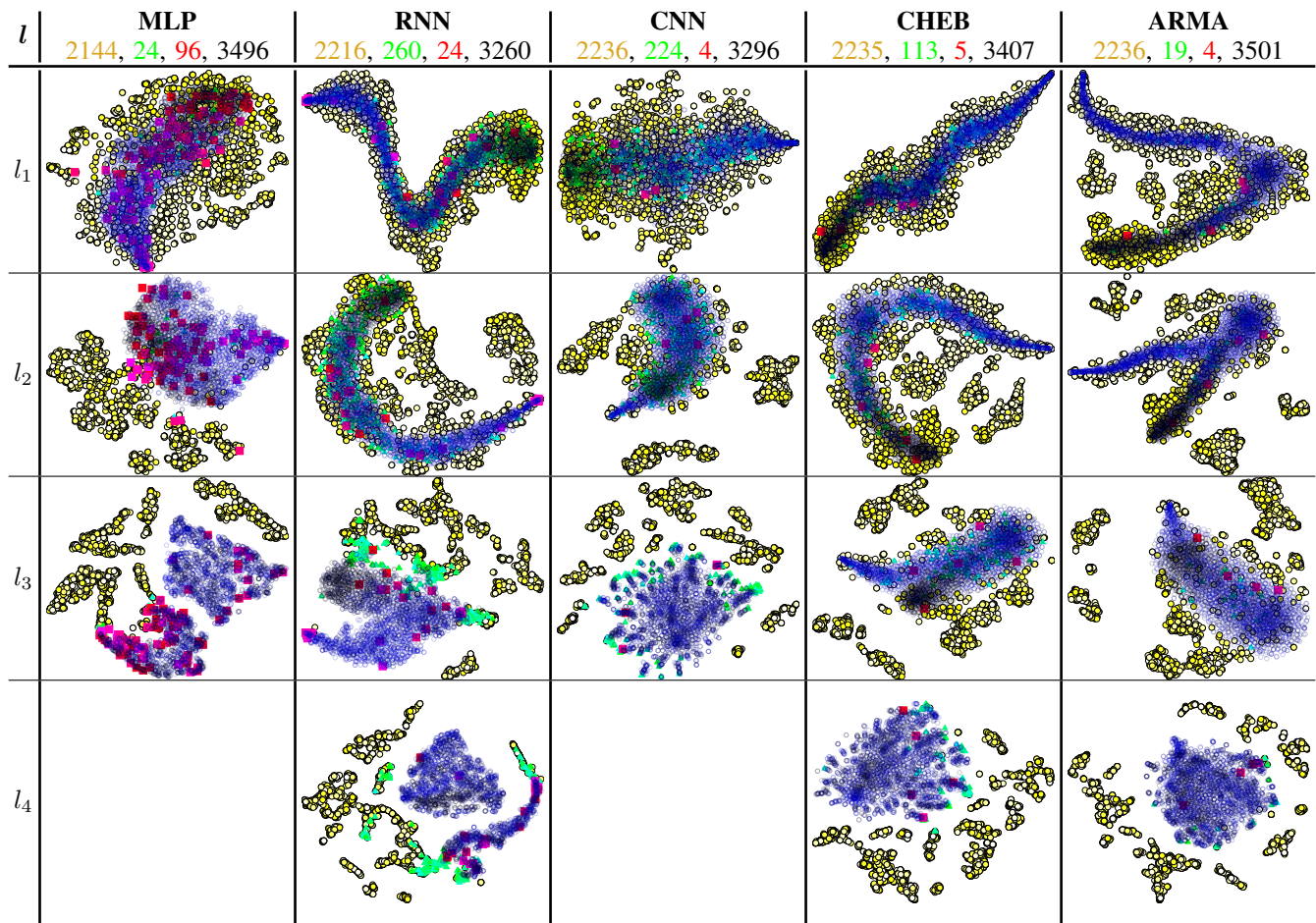


Fig. 5. t-SNE embedding of model's layers to visualize the attack detection where color encoding and embedding of true input and output data are given in Fig. 4. For each model and each layer l , output of the model is embedded in 2D using t-SNE. Since t-SNE preserve the structure of the high dimensional data, models' transformation can be visualized and compared in a lower dimension, such as 2D. Note that due to its topology aware ARMA convolutional graph filtering, the proposed model better classifies samples by converging to the true output depicted in Fig. 4d. As a consequence, it yields minimum number of FP and FN negatives compared to other models.

- [15] C. M. Bishop, *Pattern recognition and machine learning*. Springer, 2006.
- [16] Y. LeCun, Y. Bengio, and G. Hinton, "Deep learning," *nature*, vol. 521, no. 7553, pp. 436–444, 2015.
- [17] A. Ortega, P. Frossard, J. Kovačević, J. M. Moura, and P. Vandergheynst, "Graph signal processing: Overview, challenges, and applications," *Proceedings of the IEEE*, vol. 106, no. 5, pp. 808–828, 2018.
- [18] O. Boyaci, A. Umunnakwe, A. Sahu, M. R. Narimani, M. Ismail, K. Davis, and E. Serpedin, "Graph neural networks based detection of stealth false data injection attacks in smart grids," 2021.
- [19] M. Defferrard, X. Bresson, and P. Vandergheynst, "Convolutional neural networks on graphs with fast localized spectral filtering," in *Advances in Neural Information Processing Systems (NIPS)*, 2016.
- [20] N. Tremblay, P. Gonçalves, and P. Borgnat, "Design of graph filters and filterbanks," in *Cooperative and Graph Signal Processing*. Elsevier, 2018, pp. 299–324.
- [21] J. C. Mason and D. C. Handscomb, *Chebyshev polynomials*. CRC press, 2002.
- [22] S. W. Smith *et al.*, *The scientist and engineer's guide to digital signal processing*. California Technical Pub. San Diego, 1997, vol. 14.
- [23] A. Loukas, A. Simonetto, and G. Leus, "Distributed autoregressive moving average graph filters," *IEEE Signal Processing Letters*, vol. 22, no. 11, pp. 1931–1935, 2015.
- [24] F. M. Bianchi, D. Grattarola, L. Livi, and C. Alippi, "Graph neural networks with convolutional arma filters," *IEEE Transactions on Pattern Analysis and Machine Intelligence*, 2021.
- [25] X. Shi, H. Feng, M. Zhai, T. Yang, and B. Hu, "Infinite impulse response graph filters in wireless sensor networks," *IEEE Signal Processing Letters*, vol. 22, no. 8, pp. 1113–1117, 2015.
- [26] A. Loukas, M. Zuniga, M. Woehle, M. Cattani, and K. Langendoen, "Think globally, act locally: On the reshaping of information landscapes," in *Proceedings of the 12th international conference on Information processing in sensor networks*, 2013, pp. 265–276.
- [27] The Electric Reliability Council of Texas (ERCOT). Backcasted (actual) load profiles - historical. (2020, May 10). [Online]. Available: <http://www.ercot.com/mktinfo/loadprofile/alp/>
- [28] M. Abadi, P. Barham, J. Chen, Z. Chen, A. Davis, J. Dean, M. Devin, S. Ghemawat, G. Irving, M. Isard *et al.*, "Tensorflow: A system for large-scale machine learning," in *12th {USENIX} symposium on operating systems design and implementation ({OSDI} 16)*, 2016, pp. 265–283.
- [29] L. Thurner, A. Scheidler, F. Schäfer, J.-H. Menke, J. Dollichon, F. Meier, S. Meinecke, and M. Braun, "pandapower - an open-source python tool for convenient modeling, analysis, and optimization of electric power systems," *IEEE Transactions on Power Systems*, vol. 33, no. 6, pp. 6510–6521, 2018.
- [30] F. Pedregosa, G. Varoquaux, A. Gramfort, V. Michel, B. Thirion, O. Grisel, M. Blondel, P. Prettenhofer, R. Weiss, V. Dubourg *et al.*, "Scikit-learn: Machine learning in python," *the Journal of machine Learning research*, vol. 12, pp. 2825–2830, 2011.
- [31] L. v. d. Maaten and G. Hinton, "Visualizing data using t-sne," *Journal of machine learning research*, vol. 9, no. Nov, pp. 2579–2605, 2008.
- [32] A. Jindal, A. Dua, K. Kaur, M. Singh, N. Kumar, and S. Mishra, "Decision tree and svm-based data analytics for theft detection in smart grid," *IEEE Transactions on Industrial Informatics*, vol. 12, no. 3, pp. 1005–1016, 2016.
- [33] D. Wang, X. Wang, Y. Zhang, and L. Jin, "Detection of power grid disturbances and cyber-attacks based on machine learning," *Journal of Information Security and Applications*, vol. 46, pp. 42–52, 2019.
- [34] Y. Wang, M. M. Amin, J. Fu, and H. B. Moussa, "A novel data analytical approach for false data injection cyber-physical attack mitigation in smart grids," *IEEE Access*, vol. 5, pp. 26 022–26 033, 2017.
- [35] T. O'Malley, E. Bursztein, J. Long, F. Chollet, H. Jin, L. Invernizzi *et al.*, "Keras Tuner," <https://github.com/keras-team/keras-tuner>, 2019.